Spin-valve giant magneto-resistance film with magnetostrictive FeSiB amorphous layer and its application to strain sensors

Y. Hashimoto, N. Yamamoto, T. Kato, D. Oshima, and S. Iwata

Citation: Journal of Applied Physics **123**, 113903 (2018); doi: 10.1063/1.5018467
View online: https://doi.org/10.1063/1.5018467
View Table of Contents: http://aip.scitation.org/toc/jap/123/11
Published by the American Institute of Physics

Spin-valve giant magneto-resistance film with magnetostrictive FeSiB amorphous layer and its application to strain sensors

Y. Hashimoto,[1] N. Yamamoto,[1] T. Kato,[1] D. Oshima,[2] and S. Iwata[2]
[1]*Department of Electrical Engineering and Computer Science, Nagoya University, Nagoya, Aichi, Japan*
[2]*Institute of Materials and Systems for Sustainability, Nagoya University, Nagoya, Aichi, Japan*

(Received 7 December 2017; accepted 26 February 2018; published online 19 March 2018)

Giant magneto-resistance (GMR) spin-valve films with an FeSiB/CoFeB free layer were fabricated to detect applied strain in a GMR device. The magnetostriction constant of FeSiB was experimentally determined to have 32 ppm, which was one order of magnitude larger than that of CoFeB. In order to detect the strain sensitively and robustly against magnetic field fluctuation, the magnetic field modulation technique was applied to the GMR device. It was confirmed that the output voltage of the GMR device depends on the strain, and the gauge factor $K = 46$ was obtained by adjusting the applied DC field intensity and direction. We carried out the simulation based on a macro-spin model assuming uniaxial anisotropy, interlayer coupling between the free and pin layers, strain-induced anisotropy, and Zeeman energy, and succeeded in reproducing the experimental results. The simulation predicts that improving the magnetic properties of GMR films, especially reducing interlayer coupling, will be effective for increasing the output, i.e., the gauge factor, of the GMR strain sensors. *Published by AIP Publishing.* https://doi.org/10.1063/1.5018467

I. INTRODUCTION

Giant magneto-resistance (GMR) and tunnel magneto-resistance (TMR) films are used as sensitive magnetic field sensors due to their significant change in resistance under the application of small magnetic fields.[1–3]

The GMR (TMR) elements consist of two ferromagnetic layers separated by a non-magnetic metallic (insulation) layer, which is referred to as a spin valve structure, and the variation of the relative angle between their magnetizations results in the large change in the resistance of the elements. The spin valve GMR and TMR were widely used as key devices in the read head of the magnetic recording and contributed to a tremendous increase in the recording density of hard disk drives. The spin valve device also has a feature capable of monolithic integration, since the GMR and TMR elements are regarded as a simple two-terminal resistance,[4] which broadens the range of its application.

In general, TMR exhibits magneto-resistance (MR) at least one order of magnitude larger than that of GMR, which is beneficial for detecting small magnetic fields. However, for the detection of extremely small fields, such as bio-magnetic fields, the area of the MR elements should be large enough to reduce the magnetic noise.[5] Also, the TMR elements in which the current flows perpendicular to the plane (CPP) require a microfabrication process that is complicated compared with the current-in-plane (CIP) GMR. In practice, the area of the TMR elements cannot be arbitrarily large due to the increase in pinholes in the tunneling barrier, whereas the GMR is effective for increasing the device size without the reduction of the MR.

Aside from the detection of the external magnetic field or the bio-magnetic field,[6–8] the GMR (TMR) is useful for detecting a mechanical strain in the film through a change of the magnetization direction of the sensing layer induced by the inverse effect of magnetostriction. Thanks to the high sensitivity of the GMR/TMR element, the MR devices are reported to be applicable to strain gauges that are smaller in size and more sensitive[9–16] compared with conventional strain gauges. In order to realize highly sensitive GMR/TMR strain sensors, a magnetic layer having a large magnetostriction constant and exhibiting a soft magnetic property is required. For example, it has been reported that the spin valve GMR sensor with a permalloy sensing layer fabricated on an atomic force microscope cantilever exhibits a gauge factor of 150.[9] Moreover, for the magnetic tunnel junctions with a magnetostrictive free layer, gauge factors of 400–600 have been reported.[12,13] More recently, CoFeB/MgO/CoFeB magnetic tunnel junctions have been reported to exhibit a gauge factor of 2150.[16] These values are much larger than those of conventional metallic films with a gauge factor of 2–5. In addition to the GMR/TMR strain sensors, a giant magneto-impedance (GMI) strain sensor with a high gauge factor has been reported, although a high frequency signal is necessary to observe the GMI effect.[17]

However, a drawback of the reported GMR/TMR strain gauges, especially for those exhibiting a large gauge factor, is that the output is significantly influenced by the fluctuation of the external magnetic field. We have developed modulation-type magnetic field sensors which distinguish the signal from disturbance in the magnetic field.[18–21] In this paper, we fabricated a GMR spin valve element with an FeSiB free layer exhibiting relatively large magnetostriction and small magnetic anisotropy,[22] and applied the modulation technique to detect the strain sensitively and robustly against the magnetic field fluctuation. Figure 1 shows a schematic of the present GMR strain sensors, whose free layer magnetization direction is modulated by an AC magnetic field. A DC bias field was applied to rotate the magnetization along the hard axis (HA) of the free layer. When the AC field was applied along the

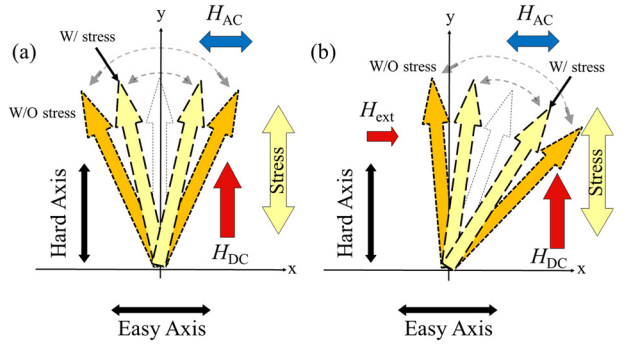

FIG. 1. Schematic of free layer magnetization of the present GMR strain sensor modulated by an AC magnetic field. The magnetization direction in the free layer is oscillated by the AC field, and the magnetization oscillation angle is modified by the application of the stress in (a). The external field applied along the easy axis does not change the AC oscillation angle but only deflects the center axis of the oscillation shown in (b).

easy axis (EA), the magnetization direction was oscillated as in Fig. 1(a). When the stress was applied to easy or hard axis, uniaxial anisotropy was induced which varied the AC oscillation angle of the free layer magnetization. However, a unidirectional magnetic field along the easy axis does not change the AC oscillation angle, but only deflects the center axis of the oscillation as shown in Fig. 1(b). This means that the unidirectional magnetic field does not influence the sensor AC output. If we use two sensors whose easy axes are perpendicular to each other, the unidirectional external field and uniaxial stress-induced anisotropy are detected independently. Here, we report the output of this type of GMR strain sensor and apply a macro-spin model to elucidate the output of the GMR strain sensors.

II. EXPERIMENTAL METHODS

The GMR film with a stack of substrate/Ta (5)/$Fe_{72}Si_{14}B_{14}$ (20)/$(Co_{90}Fe_{10})_{92}B_8$ (1.5)/Cu (2.2)/$Co_{90}Fe_{10}$ (3)/$Mn_{80}Ir_{20}$ (10)/Ta (2) was deposited using a magnetron sputtering system. The units of the layer thickness and alloy composition are nm and at. %, respectively, and the substrate is Matsunami's micro cover glass or ultrathin glass with a thickness of 0.15, 0.1, or 0.07 mm. The CoFeB (1.5) layer was inserted between the FeSiB and Cu layers to obtain a moderate MR. The GMR film with CoFeB (20) instead of the FeSiB (20)/CoFeB (1.5) double layer was also fabricated to compare the effect of the FeSiB layer with a high magnetostriction constant. In order to measure the magnetostriction constants of CoFeB and FeSiB in our GMR films, we fabricated a CoFeB single layer film with a stack of substrate/$(Co_{90}Fe_{10})_{92}B_8$ (150)/Ta (2), and an FeSiB laminated film with a stack of substrate/SiN (5)/$[Fe_{72}Si_{14}B_{14}$ (100)/SiN (5)$]_{10}$. In the case of the growth of the thick FeSiB, the laminated structure was applied for the magnetostriction measurement in order to prevent the grain growth of the FeSiB crystal, which significantly increases the magneto-crystalline anisotropy of FeSiB. The Ar pressure during the deposition was kept at 0.4 Pa. Before the deposition of the GMR films, the substrate was cleaned using 1 keV Ar^+ ion bombardment for 5 min, and during the deposition, a DC magnetic field of

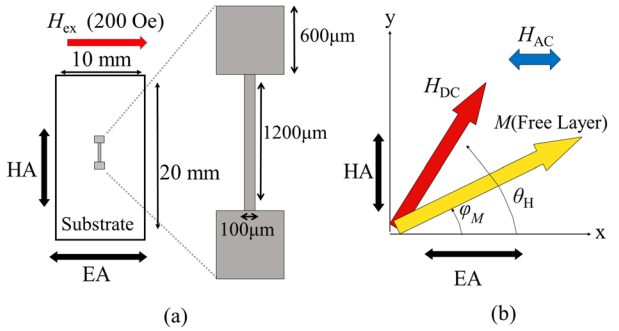

FIG. 2. (a) GMR pattern prepared on glass substrate and (b) direction of DC magnetic field H_{DC} and magnetization M from the easy axis (EA).

$H_{ex} = 200$ Oe was applied to induce uniaxial anisotropy of the GMR film.

The magnetostriction constants of the CoFeB and FeSiB films were evaluated by measuring the torque curves under application of the uniaxial strain to the film.[23,24] The MR loops of the GMR films were measured by a DC 4-point probe method in which a magnetic field is applied along the easy axis (EA) and hard axis (HA) in the film plane. The GMR films were patterned into a wire shape with a width of 100 μm and a length of 1200 μm as shown in Fig. 2(a). The microfabrication of the GMR elements was done by photolithography and Ar^+ ion etching. The easy axis of the GMR element runs along its width direction, and the external field H_{DC} was applied along θ_H from the easy axis, which tilts the magnetization of the free layer (φ_M) as shown in Fig. 2(b). The GMR element was connected to the sensor circuit to amplify the voltage due to the resistance change induced by the strain and magnetic field. Figure 3 shows a schematic of the application of the uniaxial stress to the GMR test device. The cantilever beam of the GMR device with a length of L is subjected to a vertical force at the free end, which induces the vertical deflection d at the free end. The strain ε at the position s from the fixed end is expressed as

$$\varepsilon = \frac{3dt_s(L-s)}{2L^3}, \tag{1}$$

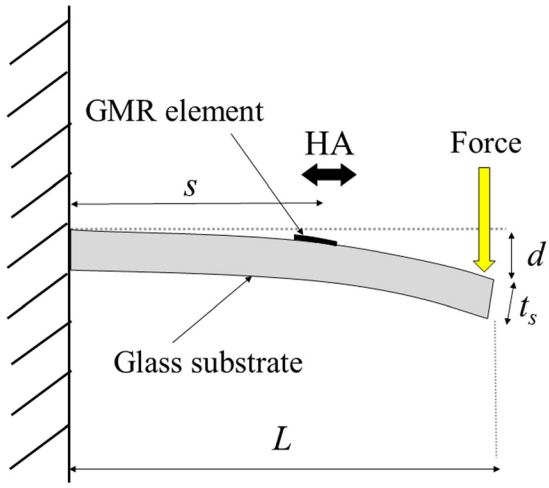

FIG. 3. Schematic of the cantilever beam of the GMR test device used to apply uniaxial strain along the hard axis of the GMR.

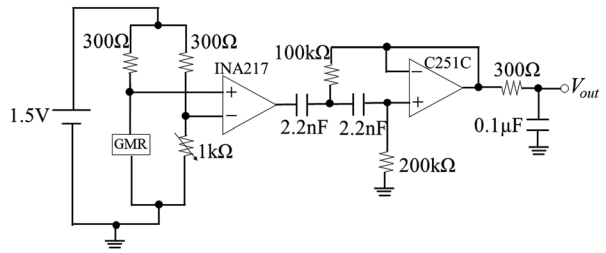

FIG. 4. Circuit for detecting the strain applied to the GMR element.

where t_s is the thickness of the substrate.[25] The strain ε induces the uniaxial magnetic anisotropy through the inverse effect of the magnetostriction. In this experiment, the uniaxial stress was applied along the hard axis (long axis) of the GMR element (Fig. 3). Figure 4 shows the signal detection circuit consisting of a bridge circuit, an instrumentation amplifier (INA217), a high-pass filter, and a low-pass filter. A bias voltage of 1.5 V was applied to the bridge circuit whose one leg contained the GMR element. The typical bias voltage applied to the GMR element was 0.77 V. The GMR device was placed at the center of four orthogonal electromagnets to apply a DC magnetic field H_{DC} in the direction of θ_H from the easy axis, as shown in Fig. 2(b), in order to rotate the free layer magnetization away from the easy axis. The additional two electromagnets were used to apply an alternating magnetic field H_{AC} (0.6 Oe rms at 1 kHz) along the easy axis as shown in Fig. 2(b) to induce harmonic oscillation of the free layer magnetization, leading to the resistance change of the GMR element at 1 kHz. The modulation of the magnetization direction is effective to reduce the DC noise of the circuit. Also, when the magnetization is oscillated around the hard axis, the oscillation amplitude becomes insensitive to the external stray field along the easy axis, which makes the sensor robust to the external field fluctuation as explained in Fig. 1. The application of the uniaxial strain along the hard axis changes the amplitude of the magnetization oscillation due to the strain-induced anisotropy, and the resultant AC component of the GMR terminal voltage is also modified by the strain-induced magnetic anisotropy field. The GMR voltage in the bridge circuit was amplified 300 times by the instrumentation amplifier, and the 1 kHz component of the amplifier output was selectively extracted by the high- and low-pass filters. The cut-off frequencies of the high- and low-pass filters were 0.512 kHz and 5.305 kHz, respectively. We defined the amplitude of the 1 kHz component of the output voltage to be V_{out}.

III. RESULTS AND DISCUSSION

A. Magnetostriction constants of $Fe_{72}Si_{14}B_{14}$ and $(Co_{90}Fe_{10})_{92}B_8$

The uniaxial strain in the CoFeB and FeSiB films was applied by pressing the substrate between a pair of sample holders whose inner surfaces have convex and concave cylinder shapes with a radius of curvature of $r = 200$ mm. The stress σ and strain ε are, respectively, expressed by the following equations:

$$\sigma = \frac{Y\varepsilon}{1+\nu}, \tag{2}$$

$$\varepsilon = \frac{t_s}{2r}, \tag{3}$$

where Y and ν are the Young's modulus and Poisson's ratio of the film, respectively. Here, we used $Y = 2.1 \times 10^{12}$ dyn/cm^2 and $\nu = 0.3$. In this experiment, the strain was estimated to be about $\varepsilon = 3.8 \times 10^{-4}$ and 1.8×10^{-4} for the CoFeB and FeSiB films, respectively. Figure 5 shows the torque curves of the CoFeB and FeSiB films under the application of tensile, L_{ten} (red), and compressive, L_{comp} (blue) stress. In addition to the stress-induced anisotropy, the torque curves L_{ten} and L_{comp} contain in-plane anisotropy of the ferromagnetic layer, background signals from the holder and sample tilting. However, the stress-induced anisotropy is selectively extracted by taking the difference between them, L_{comp}–L_{ten}, since the in-plane anisotropy and background signals are canceled by the subtraction, as shown by the green lines in Fig. 5. From the amplitude of L_{comp}–L_{ten}, the magnetostriction constant λ can be obtained using the following equation:

$$L_{comp.} - L_{ten.} = \frac{3}{2}\lambda\sigma \times 2. \tag{4}$$

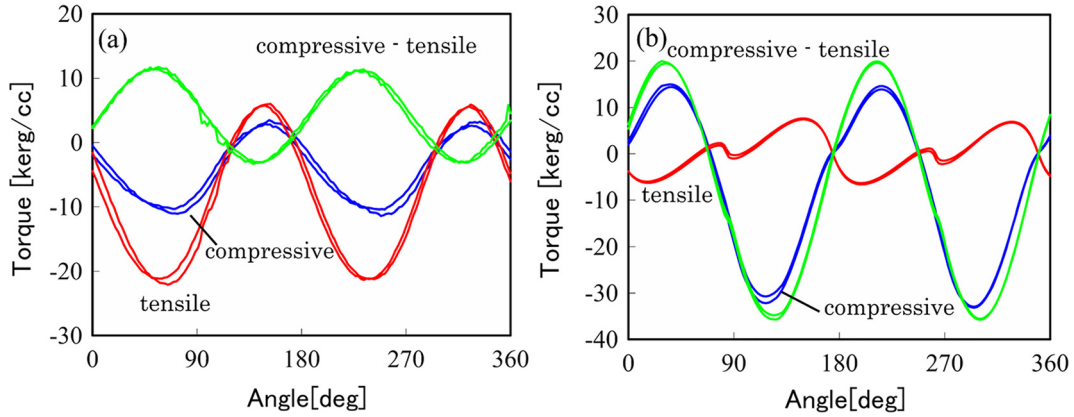

FIG. 5. Torque curves of (a) CoFeB (150) single-layer films and (b) [FeSiB (100)/SiN (5)]$_{10}$ laminated film under the application of tensile (red) and compressive (blue) stresses. The differences between the tensile and compressive stresses to eliminate the background and in-plane anisotropy of the film are shown as green lines.

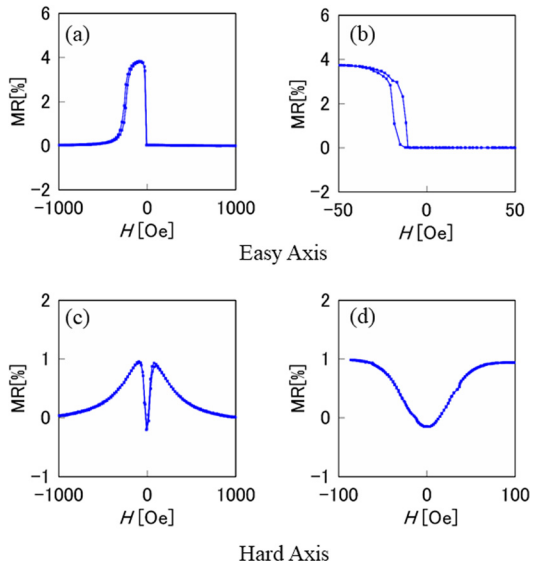

FIG. 6. MR loops along the easy axis and hard axis of the GMR films with CoFeB (20) free layers. Panels (a) and (c) are the major loops taken by applying a maximum field of 1 kOe, and panels (b) and (d) show the minor loops taken within (b) ±50 Oe and (d) ±100 Oe.

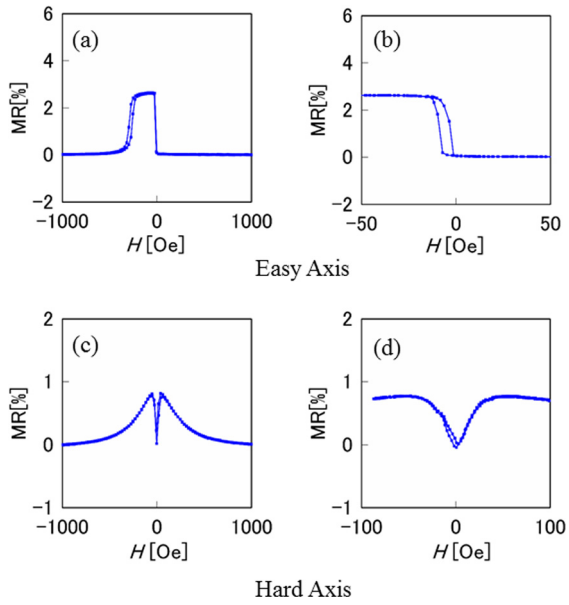

FIG. 7. MR loops along the easy axis and hard axis of the GMR films with FeSiB (20)/CoFeB (1.5) free layers. Panels (a) and (c) are the major loops taken by applying a maximum field of 1 kOe, and panels (b) and (d) show the minor loops taken within (b) ±50 Oe and (d) ±100 Oe.

The estimated λ_{CoFeB} and λ_{FeSiB} values are +3.7 ppm and +32 ppm, respectively, indicating that FeSiB has a magnetostriction constant one order of magnitude larger than that of CoFeB.

B. Magnetoresistance characteristics of the GMR element

Figures 6 and 7 show the MR loops of GMR films with CoFeB (20) and FeSiB (20)/CoFeB (1.5) free layers, respectively. The external field was applied along the easy axis and hard axis of the GMR films. Figures 6(a) and 6(c) show the major loops, and Figs. 6(b) and 6(d) show the minor loops. The MR ratio was defined as $(R_{AP} - R_P)/R_P$. Here, R_P and R_{AP} are the resistances when the magnetizations of the free and fixed layers are parallel and antiparallel, respectively. The GMR film with the free layer CoFeB (20) showed an MR ratio of about 4% as seen in Fig. 6(a), whereas the MR ratio of the FeSiB (20)/CoFeB (1.5) free layer decreased to about 2.5% as seen in Fig. 7(a). From the minor loops in Figs. 6(b) and 7(b), the loop shift of the free layer is estimated to be 15 and 5 Oe for the GMR films with CoFeB and FeSiB/CoFeB free layers, respectively. The loop shift indicates the existence of the interlayer coupling through the Cu layer, which will be originated from the magneto-static orange peel coupling[26] and the Ruderman-Kittel-Kasuya-Yoshida (RKKY) coupling.[27]

C. Output signals from GMR devices under the application of strain

Figure 8 shows the waveforms obtained from the GMR devices with CoFeB (20) [Figs. 8(a) and 8(b)] and FeSiB (20)/CoFeB (1.5) free layers [Figs. 8(c) and 8(d)]. The external field $H_{DC} = 10$ Oe was applied along the hard axis ($\theta_H = 90°$). In order to avoid the domain formation in the free layer, we first applied H_{DC} along the easy axis to saturate the free layer, then rotated H_{DC} along the direction at θ_H [see Fig. 2(b)]. The waveforms of V_{out} were taken at the output of the filter circuit, and the displacement of the cantilever end was set at $d = 0$ [Figs. 8(a) and 8(c)] and $d = 0.1$ mm

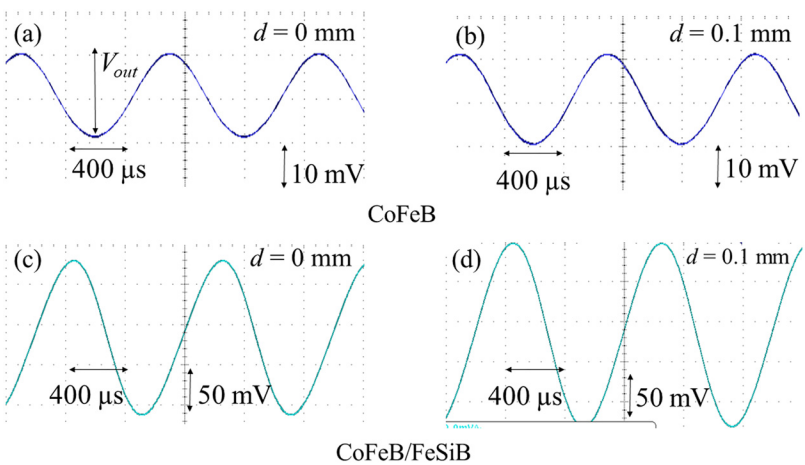

FIG. 8. Waveforms obtained from the GMR devices with (a), (b) CoFeB (20) and (c), (d) FeSiB (20)/CoFeB (1.5) free layers. The external field $H_{DC} = 10$ Oe was applied along the hard axis $\theta_H = 90°$. The displacement of the cantilever end was set at (a), (c) $d = 0$ mm and (b), (d) $d = 0.1$ mm.

[Figs. 8(b) and 8(d)]. The waveforms of the GMR outputs show a sinusoidal signal at a frequency of 1 kHz since the free layer magnetization oscillates at 1 kHz due to the alternating field H_{AC}. From Figs. 8(a) and 8(b), the peak to peak value V_{out} was 20 mV for the GMR with a CoFeB free layer, and a slight increase in V_{out} around 1 mV was observed when the deflection of the beam was changed from $d=0$ to 0.1 mm. In the case of the GMR film with an FeSiB/CoFeB free layer, the V_{out} was estimated to be 192 mV, and it increased to 229 mV when a beam deflection of $d=0.1$ mm was applied. The reason that a large V_{out} at $d=0$ was observed for the GMR with FeSiB/CoFeB compared with that with CoFeB was the small anisotropy field H_k of FeSiB/CoFeB. The H_k of the GMR element with a CoFeB free layer was 9 Oe, while H_k for the FeSiB/CoFeB free layer was 3.5 Oe. (Note that the H_k of the patterned GMR elements is different from that of the corresponding GMR films, since there exists an additional shape anisotropy in the GMR element.)

Figure 9 shows the dependence of the output voltage V_{out} on the strain ε measured for the GMR devices with (a) CoFeB and (b) FeSiB/CoFeB free layers. The external field H_{DC} was applied along the hard axis $\theta_H=90°$ and the intensity was varied from 10 to 50 Oe. As seen in Fig. 9(b), the V_{out} from the GMR device with an FeSiB/CoFeB free layer has a maximum at a certain strain ε, and the peak position shifts from positive to negative with increasing H_{DC}. This trend is not clearly seen in the GMR device with a CoFeB free layer, but the slope of the V_{out} vs ε at $\varepsilon=0$ took a maximum at $H_{DC}\sim 20$ Oe and changed its sign from positive to negative at around $H_{DC}=40$ Oe. The dependence of V_{out} on ε is much larger for the GMR device with an FeSiB/CoFeB free layer than for that with a CoFeB free layer because of the large magnetostriction constant of FeSiB compared with CoFeB as discussed in Fig. 5. The peak of the V_{out} seen in Fig. 9(b) is considered to originate from the condition that the strain-induced anisotropy roughly cancels the sum of the applied H_{DC} along the hard axis and the anisotropy field H_k along the easy axis, which makes the oscillation amplitude of the free layer magnetization by H_{AC} large. With increasing H_{DC}, the strain necessary to cancel the sum of H_{DC} and H_k is changed, but the peak value of V_{out} is not sensitively dependent on H_{DC}.

In order to understand in detail the dependence of V_{out} on the strain ε, we carried out a simulation of the magnetization oscillation of the free layer under the application of H_{DC}, H_{AC}, and strain ε. The magnetic energy of the free layer is assumed to be expressed by the sum of the uniaxial anisotropy, strain-induced anisotropy, Zeeman energy due to H_{DC} and H_{AC}, and interlayer coupling between the free and pinned layers as follows:

$$E=(-K_u+K_\varepsilon)\cos^2(\varphi_M)-MH_{DC}\cos(\theta_H-\varphi_M) -K_i\cos(\varphi_M)-MH_{AC}\cos(\varphi_M), \quad (5)$$

where K_u is the anisotropy constant containing the induced anisotropy due to the deposition under the field and the shape anisotropy due to the microfabrication. K_ε [$=-3\lambda\sigma/2$ as in Eq. (4)] is the magneto-elastic anisotropy constant, M is the magnetization (1000 emu/cc), and K_i is the anisotropy due to interlayer coupling between the pin and free layers. Here, we assumed that the magnetization of the fixed layer does not change its direction under the application of H_{DC}, H_{AC}, etc. By dividing Eq. (5) by the magnetization M, i.e.,

$$\frac{E}{M}=\frac{1}{2}(H_\varepsilon-H_k)\cos^2(\varphi_M)-H_{DC}\cos(\theta_H-\varphi_M) -H_i\cos(\varphi_M)-H_{AC}\cos(\varphi_M), \quad (6)$$

we can roughly estimate the stable direction of M using the sum of the equivalent fields. The anisotropy field H_k and the coupling field H_i are given by $H_k=2K_u/M$ and $H_i=K_i/M$, respectively, and the magneto-elastic anisotropy field H_ε is given by

$$H_\varepsilon=\frac{3\lambda Y}{M(1+\nu)}\varepsilon. \quad (7)$$

When the positive (tensile) or negative (compressive) strain is applied to $Fe_{72}Si_{14}B_{14}$ with a positive magnetostriction constant along the hard axis direction of the GMR element, the H_ε is induced in the direction of the hard axis or the easy axis, respectively. To simulate the V_{out} based on the

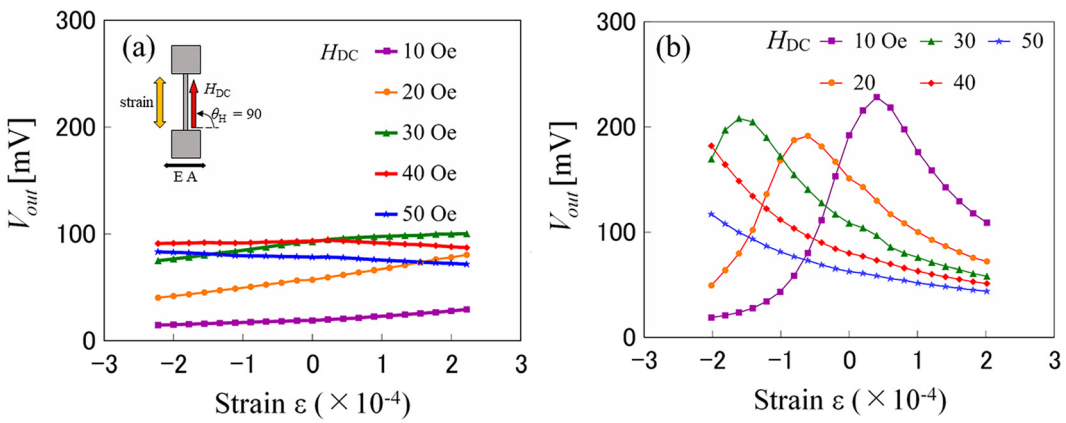

FIG. 9. Dependence of output voltage V_{out} on the applied strain ε to GMR devices with (a) CoFeB and (b) FeSiB/CoFeB free layers. The external field H_{DC} was applied along the hard axis $\theta_H=90°$ and the intensity was varied from 10 to 50 Oe.

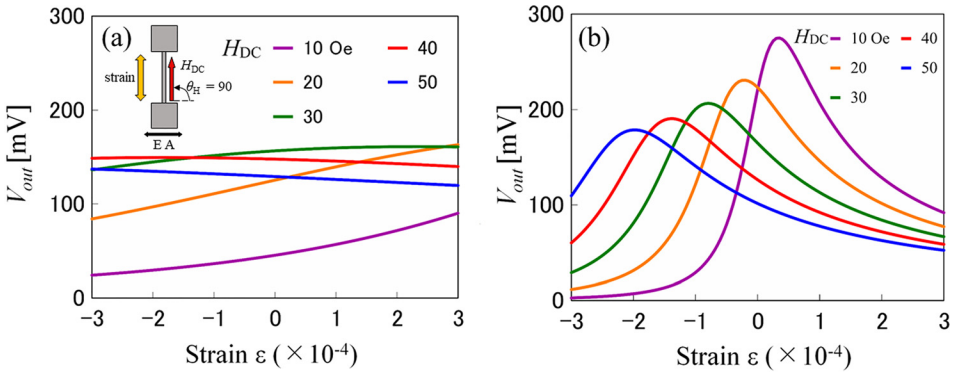

FIG. 10. Simulated output voltage V_{out} as a function of the applied strain ε to the GMR cantilever devices with (a) CoFeB and (b) FeSiB/CoFeB free layers under various H_{DC} values from 10 to 50 Oe at $\theta_H = 90°$.

model of Eq. (6), the parameters H_k and H_i were first evaluated using the resistance of the GMR elements under the application of H_{DC} at angles from $\theta_H = 30°$ to 150° without applying the strain ε and the AC magnetic field H_{AC}. Here, we assume that the magnetization of the pin layer is fixed in the direction of the easy axis. The H_k and H_i for the GMR film with an FeSiB/CoFeB free layer were estimated to be $H_k = 3.5$ Oe and $H_i = 5.5$ Oe by parameter fitting from the model of Eq. (6). H_i roughly agrees with the shift of the MR loop shown in Fig. 7(b). The GMR output V_{out} was calculated from the stable magnetization direction φ_M in Eq. (6) at the time that the waveform of H_{AC} took the maximum and minimum, φ_{max} and φ_{min}, respectively. When the bias voltage of the GMR element and the gain of the instrumentation amplifier are V and G, respectively, the V_{out} is expressed as

$$V_{out} = \frac{V}{2}(MR)G\{\cos(\varphi_{min}) - \cos(\varphi_{max})\}, \tag{8}$$

where (MR) is the maximum MR ratio of the GMR element.

Figure 10 shows the simulated V_{out} as a function of the applied strain ε for the GMR cantilever devices with (a) CoFeB and (b) FeSiB/CoFeB free layers under various DC fields H_{DC} from 10 to 50 Oe at $\theta_H = 90°$. By comparing Figs. 9 and 10, the simulated results roughly reproduce the experimental results. In the GMR device having a CoFeB free layer, both the experimental and simulated results showed positive slopes at $H_{DC} = 10$ and 20 Oe and negative slopes at $H_{DC} = 40$ and 50 Oe. In the case of $H_{DC} = 30$ Oe, a gentle peak could be confirmed around $\varepsilon = 2 \times 10^{-4}$. In the other cases, no peak appears in the range ε of $-3 \times 10^{-4} \sim 3 \times 10^{-4}$ since the magnetostriction constant of CoFeB is small.

In the case of the GMR device with an FeSiB/CoFeB free layer, the dependence of V_{out} on ε is much larger than for the device having a CoFeB free layer. There are peaks in the V_{out} vs ε in Fig. 10(b), and the peak position shifted in the negative direction with increasing H_{DC}, which coincides well with the experimental results. In the simulation, a maximum V_{out} of ~280 mV was obtained at the strain $\varepsilon = 3 \times 10^{-5}$ for $H_{DC} = 10$ Oe. At this point, the effective anisotropy field $(H_\varepsilon - H_k)$ is roughly compensated for by H_{DC}, which makes the magnetization oscillation by H_{AC} large. As H_{DC} increases, the stress-induced anisotropy field H_ε to compensate for H_{DC} also increases, which results in the shift of the peak position in the negative direction of strain ε.

In order to find a condition under which the value of V_{out} is much larger than in Fig. 9, the direction of the applied field θ_H was varied from 30° to 150°. Figure 11 shows (a) the experimental and (b) simulated ε dependence of GMR output V_{out} under the DC field $H_{DC} = 10$ Oe at various θ_H values from 30° to 150°. As shown in Fig. 11(a), a large $V_{out} \sim 700$ mV was obtained around the strain $\varepsilon = 0$ when $H_{DC} = 10$ Oe was applied in $\theta_H = 120°$, and the application of both positive and negative strains significantly reduced V_{out}. These results suggest that the x and y components of the H_{DC} roughly canceled the interlayer coupling H_i and the effective anisotropy field $(H_\varepsilon - H_k)$ at the peak position, respectively, thereby enhancing the oscillation of M under H_{AC}. The gauge factor of the sensor was estimated from the slope of V_{out} vs ε as follows:

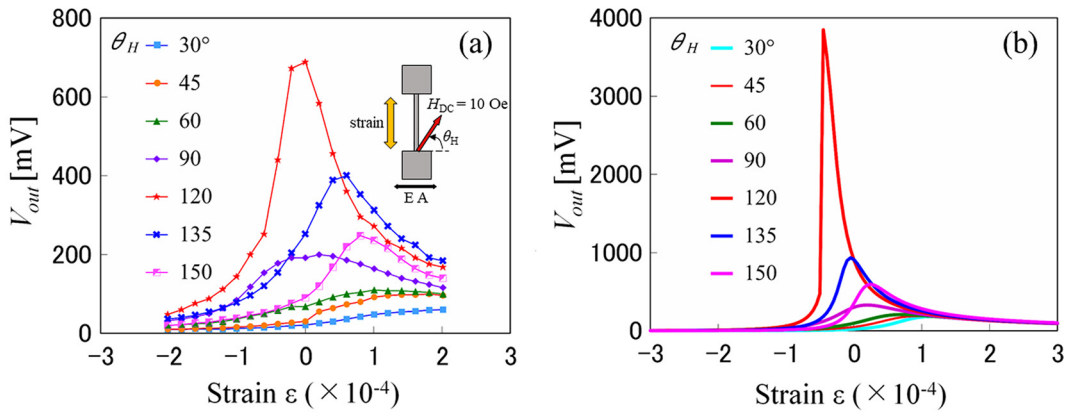

FIG. 11. (a) Experimental and (b) simulated θ_H dependence of the output voltage V_{out} under $H_{DC} = 10$ Oe at various values of θ_H from 30° to 150°.

$$K = \frac{\frac{\Delta V}{GV}}{\varepsilon}. \quad (9)$$

$\Delta V_{out}/\varepsilon$ was estimated to be 1.36×10^4 around $\varepsilon = -5 \times 10^{-5}$ for $\theta_H = 120°$, and by using a bias voltage $V = 0.77$ V and a gain $G = 300$, the gauge factor $K = 46$ was obtained.

The experimental results are reproduced qualitatively by the simulation based on Eq. (6) as shown in Fig. 11. A large V_{out} was also seen in the simulated result at $\theta_H = 120°$. However, the peak voltage of V_{out} obtained in the simulation was much larger than the experimental value. One of the reasons for the discrepancy between the experiment and simulation was considered to be the distribution of the magnetic properties in the GMR film. The free layer of the GMR film deposited under the magnetic field is considered to have the intensity and angular distributions of the uniaxial anisotropy. Moreover, the roughness of the spin valve and the thickness distribution of the Cu spacer will result in the variation of orange peel coupling and RKKY coupling between the free and pin layers, respectively. Then, we introduced the dispersion of the H_k direction and the distribution of the H_i value into the simulation. We also investigated the effect of the distribution of the H_k value in the simulation, but there was little effect on the simulated V_{out} at $\theta_H = 120°$. Figure 12 shows the assumed (a) angular distribution of H_k and (b) intensity distribution of H_i. Both are assumed to have Gaussian distributions, and the standard deviations for the direction of H_k and the intensity of H_i were set at 6° and 0.5 Oe, respectively. We calculated V_{out} at various combinations of H_k direction and H_i value using Eqs. (6) and (8), and weighted-averaged based on the profiles in Fig. 12 to calculate V_{out} from the GMR device with these distributions.

Figure 13 shows the simulated results of V_{out} from the GMR device assuming the directional dispersion of H_k and intensity distribution of H_i shown in Fig. 12. The overall tendency of the dependence of V_{out} on ε under various values of θ_H was similar to that in Fig. 11(b), but the maximum V_{out} was significantly reduced by including the distribution of the magnetic properties of the GMR film. Therefore, the distribution of the magnetic properties of GMR films is considered to be one of the reasons that V_{out} is reduced compared with the ideal case. The simulated results shown in Fig. 13 still exhibited a V_{out} value 2–3 times larger than the experiments shown in Fig. 11(a). The formation of the domains in the free layer may reduce the sensor output V_{out}, although we paid special attention to avoiding the domain formation in

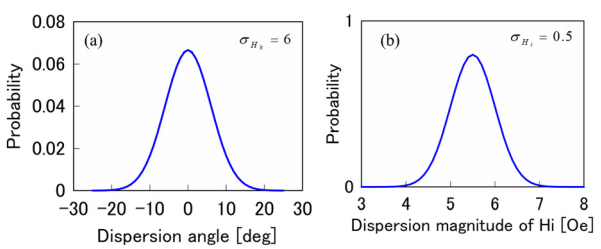

FIG. 12. (a) Assumed angular distribution of H_k having the standard deviations σ_{H_k} of 6° and (b) assumed intensity distribution of H_i having the standard deviations σ_{H_i} of 0.5 Oe.

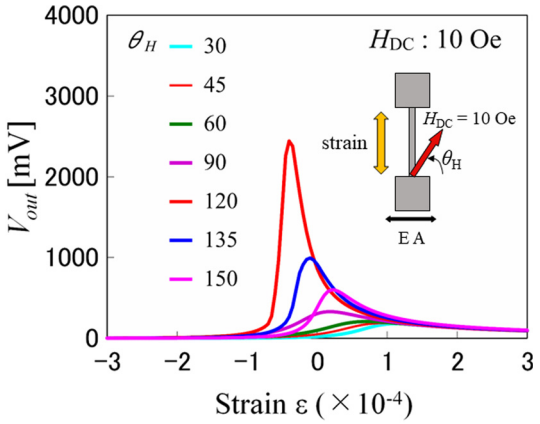

FIG. 13. Simulated results of output voltage V_{out} as a function of the applied strain ε under $H_{DC} = 10$ Oe and various values of θ_H from 30° to 150° assuming the directional dispersion of H_k and the intensity distribution of H_i in the GMR film shown in Fig. 11.

the free layer as mentioned in Fig. 9. In Fig. 13, we included both distributions, the H_k direction and H_i intensity, but the H_i distribution made the dominant contribution to reducing V_{out} (not shown here). Thus, the improvement of the magnetic properties of GMR films, especially the reduction of interlayer coupling, will be effective to increase the output, i.e., the gauge factor of the GMR strain sensors. The interlayer coupling will be reduced by improving the flatness of the spin-valve to reduce the orange peel coupling as well as the precise control of the Cu thickness to adjust the RKKY interaction between the free and pin layers.

IV. CONCLUSIONS

We fabricated a GMR spin valve with a magnetostrictive FeSiB free layer and applied a modulation technique to detect strain sensitively and robustly against the magnetic field fluctuation. The magnetostriction constants of $(Co_{90}Fe_{10})_{92}B_8$ and $Fe_{72}Si_{14}B_{14}$ used as free layers in our GMR devices were measured with a torque magnetometer and confirmed to be +3.7 ppm and +32 ppm, respectively. Two kinds of GMR films with $(Co_{90}Fe_{10})_{92}B_8$ (20 nm) and $Fe_{72}Si_{14}B_{14}$ (20 nm)/$(Co_{90}Fe_{10})_{92}B_8$ (1.5 nm) free layers were compared and confirmed to show sensitive strain detection using GMR with an FeSiB/CoFeB free layer due to the large magnetostriction constant of FeSiB. We also performed a simulation assuming uniaxial anisotropy, interlayer coupling, strain-induced anisotropy, and Zeeman energy to elucidate the dependence of the output signal voltage V_{out} on the strain ε. The overall tendency of the experimental results was reproduced by the simulation, but the simulated results had much larger V_{out} values compared with the experiments. By assuming a model including the angular dispersion of the anisotropy field and the intensity distribution of the interlayer coupling, we found that the distribution of the magnetic properties of GMR films was one of the reasons for the reduction of V_{out} in the experiment. Thus, the improvement of the magnetic properties of GMR films, especially the reduction of interlayer coupling, will be effective for increasing the output, i.e., the gauge factor of the GMR strain sensors.

ACKNOWLEDGMENTS

The authors thank Mr. M. Kumazawa of Nagoya University for his assistance with the experiments. The authors are grateful for the financial support of JSPS KAKENHI Grant Nos. 16H04328, 16K18091, 17H03249, and 17K18878. A part of this work was conducted at the Nagoya University Nanofabrication Platform, supported by the "Nanotechnology Platform Program" of the Ministry of Education, Culture, Sports, Science and Technology (MEXT), Japan.

[1]M. N. Baibich, J. M. Borote, A. Fert, F. Nguyan Van Dau, F. Petroff, P. Eitenne, G. Creuzet, A. Friederich, and J. Chazelas, Phys. Rev. Lett. **61**, 2472 (1988).
[2]T. Miyazaki and N. Tezuka, J. Magn. Magn. Mater. **139**, L231–L234 (1995).
[3]J. S. Moodera and L. R. Kinder, J. Appl. Phys. **79**, 4724 (1996).
[4]P. Ripka, *Magnetic Sensors and Magnetimeters* (Artech House, Inc., 2000), pp. 150–169.
[5]P. P. Freitas, R. Ferreira, S. Cardoso, and F. Cardoso, J. Phys.: Condens. Matter **19**, 165221 (2007).
[6]H. A. Ferreira, D. L. Graham, P. P. Freitas, and J. M. S. Cabral, J. Appl. Phys. **93**, 7281 (2003).
[7]G. Li, V. Joshi, R. L. White, S. X. Wang, J. T. Kemp, C. Webb, R. W. Davis, and S. Sun, J. Appl. Phys. **93**, 7557 (2003).
[8]S. C. Mukhopadhyay, K. Chomsuwan, C. P. Gooneratne, and S. Yamada, IEEE Sens. J. **7**, 401 (2007).
[9]H. J. Mamin, B. A. Gurney, D. R. Wilhoit, and V. S. Speriosu, Appl. Phys. Lett. **72**, 3220 (1998).
[10]T. Duenas, A. Sehrbrock, M. Lohndorf, A. Ludwig, J. Wecker, P. Grunberg, and E. Quandt, J. Magn. Magn. Mater. **242–245**, 1132–1135 (2002).
[11]M. Lohndorf, T. A. Duenas, A. Ludwig, M. Ruhrig, J. Wecker, D. Burgler, P. Grunberg, and E. Quandt, IEEE Trans. Magn. **38**(5), 2826–2828 (2002).
[12]M. Lohndorf, T. Duenas, M. Tewes, E. Quandt, M. Ruhrig, and J. Wecker, Appl. Phys. Lett **81**, 313 (2002).
[13]M. Lohndorf, S. Dokupil, J. Wecker, M. Ruhrig, and E. Quandt, J. Magn. Magn. Mater. **272–276**, 2023–2024 (2004).
[14]T. Uhrmann, L. Bar, T. Dimopoulos, N. Wiese, M. Ruhrig, and A. Lechner, J. Magn. Magn. Mater. **307**, 209–211 (2006).
[15]S. Dokupil, M.-T. Bootsmann, S. Stein, M. Lohndorf, and E. Quandt, J. Magn. Magn. Mater. **290/291**, 795–799 (2005).
[16]A. Tavassolizadeh, K. Rott, T. Meier, E. Quandt, H. Hölscher, G. Reiss, and D. Meyners, Sens. **16**, 1902 (2016).
[17]G. Buettel, J. Joppich, and U. Hartmann, Appl. Phys. Lett **111**, 232401 (2017).
[18]G. A. Wang, S. Nakashima, S. Arai, T. Kato, and S. Iwata, J. Appl. Phys. **107**, 09E709 (2010).
[19]G. A. Wang, Y. Masuda, T. Kato, and S. Iwata, J. Phys. D: Appl. Phys. **43**, 455001 (2010).
[20]G. A. Wang, Y. Masuda, T. Kato, and S. Iwata, J. Appl. Phys. **109**, 07E523 (2011).
[21]G. A. Wang, S. Arai, T. Kato, and S. Iwata, J. Phys. D: Appl. Phys. **44**, 235003 (2011).
[22]Y. Suwa, S. Agatsuma, S. Hashi, and K. Ishiyama, IEEE Trans. Magn. **46**, 666 (2010).
[23]S. Tsunashima, H. Takagi, K. Kamegaki, T. Fujii, and S. Uchiyama, IEEE Trans. Magn **14**(5), 844 (1978).
[24]H. Takahashi, S. Tsunashima, S. Iwata, and S. Uchiyama, Jpn. J. Appl. Phys., Part 2 **32**, L1328 (1993).
[25]I. Taher, M. Aslam, M. A. Tamor, T. J. Potteer, and R. C. Elder, Sens. Actuators, A **45**, 35–43 (1994).
[26]B. D. Schrag, A. Anguelouch, S. Ingvarsson, G. Xiao, Y. Lu, P. L. Trouilloud, A. Gupta, R. A. Wanner, W. J. Gallagher, P. M. Rice, and S. S. P. Parkin, Appl. Phys. Lett. **77**, 2373 (2000).
[27]S. S. P. Parkin, R. Bhadra, and K. P. Roche, Phys. Rev. Lett. **66**, 2152 (1991).